communications materials

Article

https://doi.org/10.1038/s43246-024-00494-4

Metallic local-moment magnetocalorics as a route to cryogenic refrigeration

Thomas Gruner[1,4] ✉, Jiasheng Chen[1], Dongjin Jang[2], Jacintha Banda[3], Christoph Geibel[3], Manuel Brando[3] & F. Malte Grosche[1] ✉

Commercial adiabatic demagnetisation refrigerators still employ the same hydrated salts that were first introduced over 85 years ago. The inherent limitations of these insulating magnetocalorics – poor thermal conductivity at sub-Kelvin temperatures, low entropy density, corrosiveness – can be overcome by a new generation of rare-earth based metallic magnetocalorics. Here, we present the metallic magnetocaloric $YbNi_{1.6}Sn$ as an attractive alternative to conventional refrigerants. $YbNi_{1.6}Sn$ retains high entropy into the 100 mK regime and avoids the noble metal constituents of alternative refrigerants. Demagnetisation tests demonstrate that $YbNi_{1.6}Sn$ enables economical and durable alternatives to traditional cooling devices for temperatures reaching below 120 mK. We find that the magnetocaloric properties of this material are facilitated by unusually small Kondo and RKKY interactions, which position $YbNi_{1.6}Sn$ in the extreme local moment limit on the generalised Kondo lattice phase diagram.

Low temperature cooling techniques have enabled some of the most dramatic scientific discoveries in condensed matter physics[1], such as superconductivity, superfluidity, the quantum Hall effects and much more. But access to the sub-Kelvin range is no longer of interest to fundamental research alone: quantum engineering, the use of quantum effects for new technologies, relies on quiet environments, which in solid state devices implies low temperatures[2–4]. To achieve its growth potential, the burgeoning field of solid-state based quantum devices and sensors[5–7] requires compact, efficient and low-maintenance cryogenic refrigeration.

Conventional cooling techniques in the Kelvin temperature range exploit the high entropy carried by atoms, namely the helium isotopes ^{4}He and ^{3}He[8]. Cooling systems based on manipulating liquid helium—so-called *wet systems*—can offer excellent performance at the lowest temperatures but are complicated to manufacture, require gas handling systems and pumping arrangements, and suffer from the high cost of ^{3}He. They tend to be space-hungry, expensive to build and to run and difficult to operate and maintain. By contrast, adiabatic demagnetisation refrigeration (ADR) exploits the large entropy associated with local magnetic moments in a refrigerant unit by changing the applied magnetic field. ADR systems can be assembled from mass-produced components, they are compact and straightforward to operate, but they require carefully selected magnetocaloric refrigerant materials.

Current commercial ADR systems employ insulating magnetocalorics that were first identified more than 85 years ago[9–11]. In these hydrated salts and garnets, the moments are spatially diluted in order to suppress magnetic order, and their entropy density, and consequently the cooling capacity, is thereby limited[8,12]. Moreover, because these substances are insulators, their thermal conductivity freezes out at low temperature, making it challenging to achieve thermal contact. These intrinsic limitations necessitate hermetically sealed composite pills with an integral thermal bus, which are difficult to scale down.

Metallic magnetocalorics with a high density of rare-earth-based local magnetic moments may overcome these limitations, replacing conventional refrigerants in the same field and temperature range and offering the prospect of miniaturising magnetic cooling to unprecedented levels. This is of central importance in weight critical applications such as satellite deployment of quantum sensors, and it offers new design possibilities for multi-stage cooling systems.

The fundamental challenge in the search for low temperature magnetocalorics consists in identifying materials that can retain high entropy down to very low temperature. The first demonstration of demagnetisation refrigeration using a metallic magnetocaloric[13] showed that in some rare earth compounds, magnetic moments exhibit a very small mutual interaction despite the presence of itinerant carriers. Such a

[1]Cavendish Laboratory, University of Cambridge, Cambridge CB3 0HE, UK. [2]Center for Thermometry and Fluid Flow Metrology, Division of Physical Metrology, Korea Research Institute of Standards and Science (KRISS), Daejeon 34113, Republic of Korea. [3]Max Planck Institute for Chemical Physics of Solids, Nöthnitzer Straße 40, 01187 Dresden, Germany. [4]Present address: SLB Cambridge Research, High Cross, Cambridge CB3 0EL, UK. ✉e-mail: TGruner@slb.com; fmg12@cam.ac.uk

material behaves like an insulating paramagnetic salt, but with added conduction electrons that aid thermal conduction. This contrasts with materials prepared close to a magnetic quantum critical point (QCP)[14], where strong correlations may still persist that suppress the entropy. Selection principles for metallic magnetocaloric materials will be discussed below.

Here, we report the discovery and characterisation of the new intermetallic refrigerant $YbNi_{1.6}Sn$ and demonstrate its application in a prototype ADR module even under substantial heat loads. This material represents a significant improvement on conventional insulating refrigerants, because (i) its thermal conductivity at low temperature is boosted by the presence of mobile carriers, (ii) it retains high entropy S to low temperature, producing an entropy landscape $S_{total}(T, B)$ that is more favourable for operative applications than that of quantum critical magnetocalorics, and (iii) it avoids the precious metals required in other metallic magnetocalorics such as the $YbPt_2Sn$ presented in ref. 13. This, combined with the uncomplicated synthesis makes $YbNi_{1.6}Sn$ well suited for a wide range of cooling applications beyond the laboratory scale.

Results and discussion

Selection principles for metallic magnetocalorics

Metallic refrigerants intrinsically offer higher thermal conductivity at low temperature and avoid other limitations of current insulating refrigerants. However, the fundamental property of degenerate Fermi gases—and by extension of Fermi liquids—that the electronic entropy S_{elec} is strongly suppressed in proportion to the ratio of thermodynamic temperature T over Fermi temperature T_F, seems to limit useful magnetocalorics to magnetic insulators, at least for low T refrigeration. This problem can be addressed by seeking out materials with low T_F, or narrow electronic energy bands. Such materials, metals which retain high entropy down to temperatures in the Kelvin range, can be found among the large classes of rare-earth based intermetallics, in particular those containing Ce or Yb. In these so-called Kondo lattice materials, unpaired electrons in the 4*f*-shells are spatially isolated from those on neighbouring atoms by the more extended *s*, *p* and *d*-orbitals, which define the separation between the ions. The interplay between the electrons in the more localised *f*-states and those in extended states is a topic of intense research, summarised in the Doniach phase diagram shown in Fig. 1a (see, for example refs. 15–17). It is parametrised in the first instance by the electronic density of states g_0 at the Fermi level of electrons in extended *s*, *p*, and *d*-states and by their on-site exchange interaction J with electrons in the more localised *f*-states. The local exchange interaction J depends on hopping matrix elements, on the on-site Coulomb interaction and on the orbital degeneracy. Therefore, it is highly tunable, for instance by varying the composition or the lattice density. It sets the Kondo scale T_K, which in a single-impurity model follows $T_K \simeq g_0^{-1} \cdot \exp[-1/(2J \cdot g_0)]$, as well as the Ruderman-Kittel-Kasuya-Yosida (RKKY) exchange between local moments $T_{RKKY} \simeq g_0 \cdot J^2$.

To the right of the phase diagram in Fig. 1a and at temperatures below T_K, a correlated metal emerges with high effective masses of the charge carriers, so-called heavy fermions. The heavy fermion state is associated with ultra-narrow energy bands of width $\simeq k_B T_K$, which lead to a sharp peak in the density of states near the chemical potential and correspondingly high entropy down to about T_K.

For reduced J, these renormalised bands narrow further, as the associated temperature scale T_K is decreased. In calculations with a single *f*-state embedded in a simple metal, T_K approaches 0 only for $J \to 0$, but more comprehensive calculations for the Kondo lattice suggest that T_K may vanish already at finite J[18], as indicated by J_c in Fig. 1a. This can be interpreted as an interaction-driven localisation of the electrons in *f*-states only, sometimes referred to as an *orbitally selective Mott transition* or *Kondo-breakdown*. Beyond this point, coherent transport still occurs via the extended 'conduction electron' states, but the *f*-electrons are fully localised. Since their only remaining low-energy degree of freedom is their spin, they can form a spin liquid, provided magnetic order is avoided. Spin liquids support topological order and fractionalised excitations[17], and they are of profound fundamental interest[19].

This picture suggests that magnetocalorics could be found by reducing T_K, which is achieved by reducing J. The problem with this approach is that the RKKY scale T_{RKKY} does not fall as quickly as T_K and will for intermediate J induce long-range magnetic order below a transition temperature T_m. Therefore, the spin liquid state competes at low T with magnetic order (T_m-line forming a dome in Fig. 1a), which reduces the entropy (grey entropy lines in Fig. 1b, c) and thereby limits the cooling capacity. This would

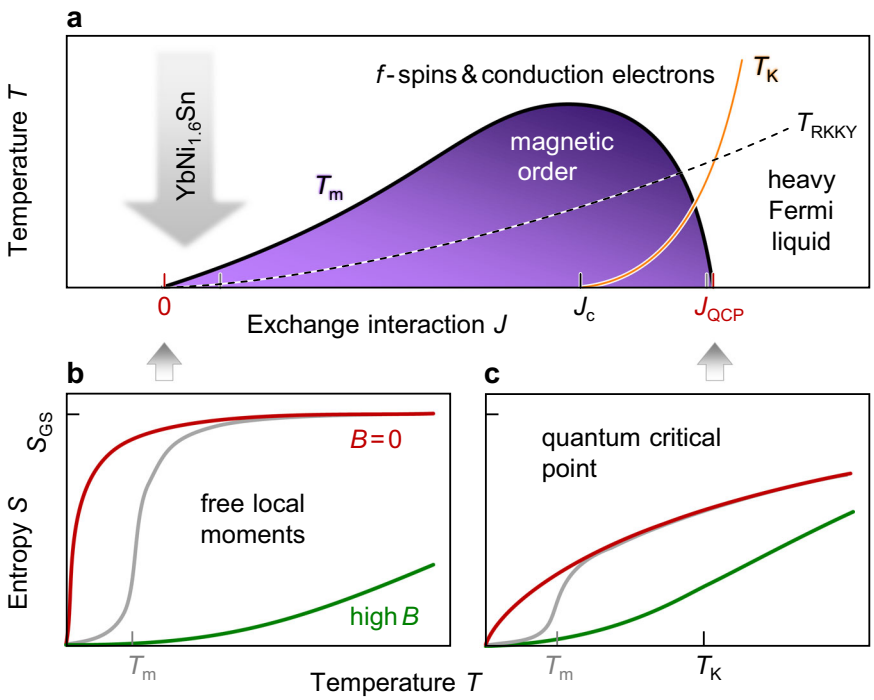

Fig. 1 | Doniach phase diagram. a Low temperature states in metallic *f*-electron materials depend on the effective exchange interaction J. This sets the Kondo scale T_K as well as the indirect exchange coupling T_{RKKY}, which induces magnetic order below T_m. **c** To the right of the T_K line, a heavy Fermi liquid forms and entropy S is suppressed below T_K. **b** As $J_K \to 0$, local moments become largely independent and can retain high but strongly field-dependent S down to very low T. This scenario appears to be realised in some Yb compounds, including $YbNi_{1.6}Sn$.

constrain the optimal position in the phase diagram to the quantum critical point at J_{QCP}, where $T_m \to 0$ but T_K may remain large. In the standard Kondo lattice picture outlined above, the quantum critical point is reached when $T_K \simeq T_{RKKY}$, which happens for $g_0 J = g_0 J_{QCP} \simeq 0.1$. The diluted quantum critical system $Yb_{0.81}Sc_{0.19}Co_2Zn_{20}$ – recently proposed as passable cooling candidate[14] – would be classified right here.

This limitation could be overcome, if the dome of magnetic order is shrunk by magnetic frustration, for instance in three-dimensional systems with face-centred cubic (fcc) or pyrochlore lattice structure[20]. As a result, the spin liquid state would now extend to low T. But this would still not produce the ideal magnetocaloric: although not frozen into static magnetic order, spins in a spin liquid are not altogether free. They are still subject to strong correlations, which again suppress the entropy at low $T < T_{RKKY}$. The two scenarios outlined so far – to seek out the heavy fermion state near the QCP where $T_m \to 0$ (Fig. 1c) or to use geometric frustration to home in on the region where $T_K \to 0$ – both suffer from the problem that the RKKY interaction T_{RKKY} remains large and suppresses the electronic entropy at sub-Kelvin temperatures. This normally shifts significant entropy towards higher temperatures (well above 2 K) and weakens the impact of the magnetic field (green curve in Fig. 1c). Magnetic fields realistic for cooling applications cannot suppress quantum critical correlations completely. Therefore, an enhanced Sommerfeld coefficient γ_0 is still observed at high fields. Furthermore, in all scenarios where T_K is relevant, the 4*f* moments are still partially Kondo-screened leading to a weaker polarisation and thereby to weaker field dependence.

Local moments. Despite these fundamental obstacles, some Yb- and Ce-based materials clearly display colossal entropy and a much more favourable field dependence. They follow essentially local-moment behaviour down to temperatures of order 0.3 K and below. These include cubic $YbPd_2Sn$[21], $YbPd_2In$[22], $YbPt_2In$[23], $YbCu_4Ni$[24] and $CePt_4Sn_2$[25] as well as hexagonal $YbPt_2Sn$[13,23]. The underlying electronic density of states in these materials is moderate, $g_0 \sim 1 - 10(\text{eV f.u.})^{-1}$, as indicated for instance by the small heat capacity jump at the superconducting transition in $YbPd_2Sn$[21]. Their vanishing T_K, ultra-low T_{RKKY} and tiny T_m, all $\ll 1$ K, are not consistent with reaching $g_0 J \sim 0.1$, required in the standard Kondo lattice picture near a quantum critical point, where T_K exceeds T_{RKKY}: for $g_0 J \simeq 0.1$ with $T_{RKKY} = g_0 J^2 \sim 0.3$ K, would require $g_0 \simeq 300$ eV/f.u., two orders of magnitude higher than the experimental values. These considerations indicate an anomalously small local exchange coupling J in these materials, which would place them all the way over to the left side of the Doniach dome, in the extreme local regime (Fig. 1b). As will be shown below, our findings in $YbNi_{1.6}Sn$ suggest that it also falls into the extreme local regime on the Doniach diagram.

The metallic refrigerant $YbNi_{1.6}Sn$

X-ray powder diffraction patterns of as-cast $YbNi_{1.6}Sn$ confirm that it crystallises in an fcc crystal structure ($Fm\bar{3}m$) with lattice parameter $a = 6.3645(2)$ Å. This is in good agreement with prior reports[26]. The refined atomic occupancy factors show a previously unreported Yb:Ni:Sn ratio of 1:1.6:1. Weak additional lines in the X-ray pattern are consistent with a minority phase of fcc $YbNi_4Sn$, confirmed in microprobe analysis. Differential scanning calorimetry and X-ray diffraction on samples with different heat treatment suggest that the functional fcc $YbNi_{1.6}Sn$ phase is meta-stable at temperatures below 1300 K. Further details on the structure of as-cast $YbNi_{1.6}Sn$, on the effects of different heat treatments and the nature of the high temperature phase transition are given in Supplementary Note 1 and 2. Nevertheless, the functional $YbNi_{1.6}Sn$ phase is long-time stable below 500 K, enabling ultra-high vacuum bake-out when required, in contrast to the traditional hydrated salt coolants, which decompose at elevated temperature. $YbNi_{1.6}Sn$ can be cast into rods or bars, provided it is quenched effectively. Sintering was also successfully tested. This makes it straightforward to form the material into the desired refrigerant pill geometry, in contrast to the procedures required for delicate hydrated salt or hard and brittle garnet refrigerants.

Measurements of the dependence of the electrical resistivity ρ on temperature demonstrate that $YbNi_{1.6}Sn$ is metallic and non-superconducting down to $T < 0.35$ K (Supplementary Note 3). Because electronic conduction contributes significantly to the low T thermal conductivity in metals[8], $YbNi_{1.6}Sn$ can reach far higher thermal conductivity than standard magnetocaloric salts or garnets in the temperature interval of interest. This removes the need for adding metal wire bundles or mesh to boost thermal contact, as is frequently done for conventional magnetocalorics[27,28], simplifies the construction of the pill, makes it easier to miniaturise pill design, minimises inactive pill volume, and thereby optimises the effective volumetric entropy capacity. Furthermore, the monotonic increase of ρ with T suggests that Kondo scattering is absent or remarkably weak. Analysing the measured magnetic properties of $YbNi_{1.6}Sn$ confirms that stable trivalent Yb^{3+} ions experience extraordinarily weak exchange interactions (Supplementary Note 4).

Specific heat. In zero applied field, the temperature dependence of the electronic contribution to the heat capacity $C_{elec}(T, B = 0)$ at low T (Fig. 2a) reveals a broadened anomaly at $T_m \approx 140$ mK, visible only after the nuclear contribution $C_n(T, B = 0)$ has been subtracted and when the electronic contribution is plotted as $C_{elec}(T)/T$ versus T (Supplementary Note 6). This tiny T_m corresponds to arguably one of the weakest magnetic interactions J in free local-moment metals found so far. Above about 0.5 K, $C(T) \propto T^{-1}$ up to $\simeq 4$ K, where it reaches a clear minimum (Fig. 2a). This power-law dependence is faster than the predicted temperature dependence for the single Kondo ion model[29] but slower than the T^{-2} form, which is the leading term expected for a lattice of local moments with intersite interactions within a high temperature series expansion[23]. Accordingly, the broad anomaly at T_m in C_{elec}/T very likely reflects short range magnetic ordering, long range order being prevented by the strong fluctuations. These data, together with the monotonic T dependence of the resistivity and the results from the low T magnetic measurements, suggest a very low or even vanishing single-impurity Kondo temperature $T_K \ll 1$ K, leading to essentially localised Yb moments, weakly coupled to the conduction electrons and to each other over most of the experimentally accessible temperature range.

At elevated temperature $T > 4$ K, lattice vibrations and excitations into higher CEF levels start to add into C, because for trivalent Yb^{3+}, the local cubic symmetry causes the eight-fold degenerate $J = 7/2$ multiplet to be split (Supplementary Note 5). In applied magnetic field, the degeneracy of the ground state doublet is lifted by the Zeeman effect as shown by the shift of broad maxima towards higher temperatures (Fig. 2a). The fact that the peaks at T_{max} – where $C_{elec}(T)$ is maximal—are broadened and flattened suggests short-range correlations between magnetic ions, which disperse the Schottky-type anomalies for two-level systems by introducing an internal field distribution. Compared to other ADR materials, the field dependence of $T = T_{max}$ is relatively strong[30] which is favourable for good cooling performance.

Electronic entropy. The entropy as shown in Fig. 2b comprises only the electronic contributions from local moments C_{4f} and conduction electrons C_{cond}, whereas the nuclear contribution C_n is subtracted out and the phonon contribution C_{ph} is neglected. Each individual C_{elec} was extrapolated from the lowest measured point to absolute zero and then integrated up: $S_{elec}(T)_B = \int_0^T (C_{elec}/T')\, dT'_B$ (Supplementary Note 6). The molar entropy S_{elec} found in this way is shown in Fig. 2b and reaches a pronounced plateau at around $R \ln 2$ in zero field, confirming that the lowest CEF level is doubly degenerate (Supplementary Note 5). This furthermore confirms our interpretation of the specific heat and indicates that our estimates of the nuclear contributions are reasonable.

The behaviour of quantum critical cooling compounds is fundamentally different in terms of their entropy evolution with temperature and field. In Fig. 3a the T dependence of S_{elec} in zero and applied field in $YbNi_{1.6}Sn$ is compared to that of the super-heavy electron material $Yb_{0.81}Sc_{0.19}Co_2Zn_{20}$ (ref. 14) and that of $YbCu_{4.6}Au_{0.4}$, which is located at

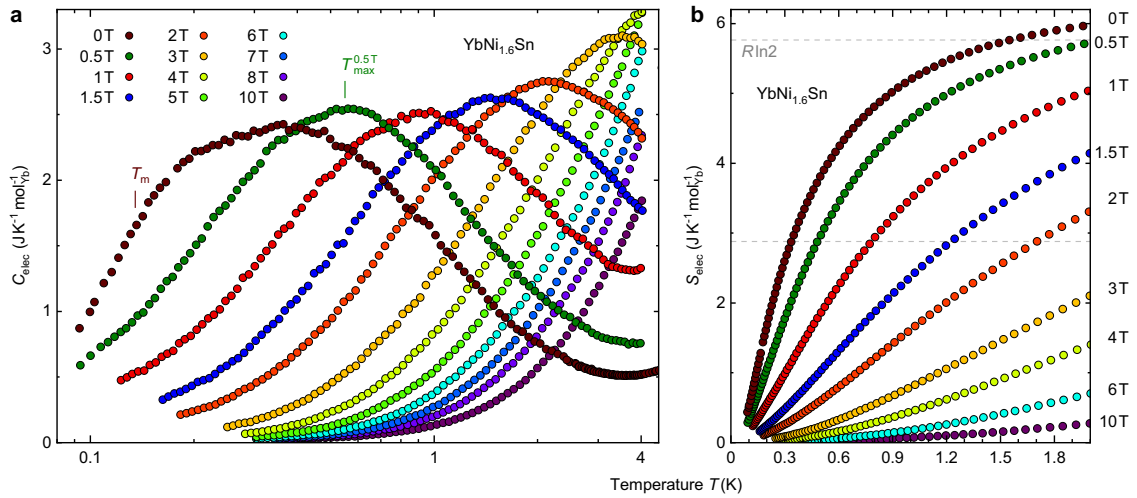

Fig. 2 | Electronic specific heat and entropy. a Temperature dependence of C_{elec} of $YbNi_{1.6}Sn$ at various magnetic fields where nuclear contributions are deducted. Although a zero field phase transition is not obvious here, deeper analyses show a broad anomaly at $T_m \approx 140$ mK. The temperature of the peak value of $C_{elec}(0.5\ T)$ is marked by $T_{max}^{0.5\ T}$ as an example. **b** The field-dependent increment of the electronic entropy S_{elec}. In zero field $S_{elec}(0\ T)$ plateaus at around $R \ln 2$ confirming a doubly degenerate ground state.

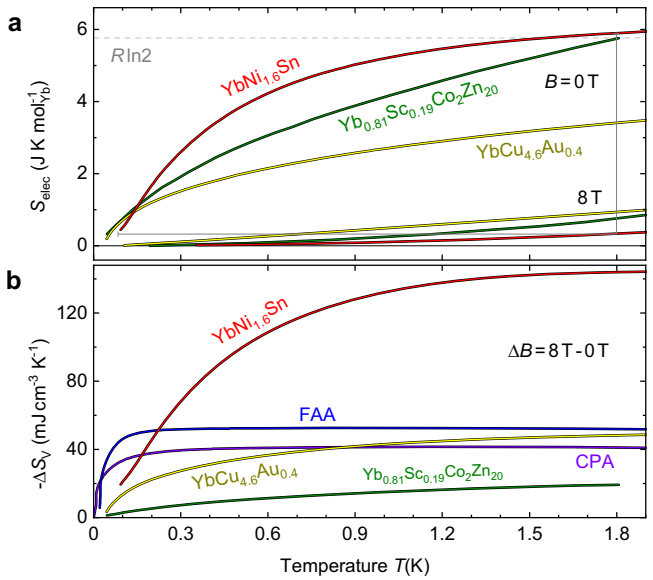

Fig. 3 | Contrasting entropies. a S_{elec} is compared for three generically different metallic magnetocalorics in zero and finite field. These are $YbNi_{1.6}Sn$ and the QCP materials $Yb_{0.81}Sc_{0.19}Co_2Zn_{20}$[14] and $YbCu_{4.6}Au_{0.4}$[31]. The process of magnetic refrigeration is shown by an orthogonal pair of solid grey lines. **b** Comparison of changes in volumetric entropy densities $-\Delta S^v(T)$ for 8 T-0 T field change, which is centrally important for application.

a QCP induced by competing AFM and FM correlations[31]. For the cooling process, the materials are first isothermally magnetised (vertical lines in Fig. 3b). The larger the entropy difference on this path, the higher the heat absorption during magnetisation and the better are the start conditions for a long hold time at base temperature in the subsequent adiabatic demagnetisation (horizontal lines in Fig. 3b). Eventually, the material tracks the $S(T, B = 0)$ line as it warms up in zero field. Figure 3a provides an impressive experimental demonstration of the difference in the entropy $S(T, B)$ landscape between QC systems and a local moment system with very weak intersite interactions. At $B = 0$, a significant part of the entropy recovery is shifted to higher T in the QC system $Yb_{0.81}Sc_{0.19}Co_2Zn_{20}$ due to the sizeable Kondo interaction. Moreover, the entropy at higher temperature and higher field (1.8 K, 8 T) is larger in the QC system, again because the Kondo interaction prevents a fully polarised state. Thus, Fig. 3a confirms the assumed $S(T, B)$ landscape presented in Fig. 1 and illustrates the limitations connected with a QC system. A very similar behaviour is also observed in the QC system $YbCu_{4.6}Au_{0.4}$[31–34] which is balanced at a magnetic QCP by frustration between AFM and FM correlations, producing a metallic 'spin liquid'. The entropy profile in these materials varies more gradually, because the magnetic entropy is distributed between $T = 0$ and T_{RKKY}, which can be much higher than the freezing/ordering temperature, i.e., well above 2 K. What makes a good metallic magnetocaloric are low energy scales $T_{RKKY} \ll 1$ K and $T_K \ll 1$ K. A QC system with such low energy scales would have an equally favourable entropy profile as $YbNi_{1.6}Sn$, but for the reasons outlined above this is difficult to achieve in currently investigated material families, some of which – like $YbNi_{1.6}Sn$ – instead appear to fall into the local moment regime.

Since magnetic transitions commonly reduce the zero field entropy, they limit the effect of magnetic refrigeration below the transition temperature T_m (generically shown in Fig. 1). This issue is most evident in $YbPd_2Sn$[21] and $YbPd_2In$[22], which undergo transitions at $T_m \approx 230$ mK and 250 mK, respectively. Although the steep slope in the entropy near T_m ensures long hold times at that temperature, it rules out base temperatures $\ll T_m$. In $YbNi_{1.6}Sn$ a transition roughly 100 mK below T_m of the reference compounds[21,22] leads to less pronounced limitations. To achieve the lowest possible base temperature, therefore, it is favourable to identify systems with super-low T_m or even completely suppressed magnetic order, like $YbNi_{1.6}Sn$ or $Yb_{0.81}Sc_{0.19}Co_2Zn_{20}$.

Entropy for magnetic refrigeration. The cooling properties of a refrigerant material are determined not just by the electronic contribution to the entropy S_{elec} but by its total entropy S_{total}, including the entropy of 4*f*-moments, valence electrons, nuclear moments and lattice. In $YbNi_{1.6}Sn$, as in many other magnetocalorics, the nuclear contribution to the specific heat becomes sizeable below ≈ 200 mK, depending on the conditions. Since during the adiabatic cooling process a decrease in the nuclear entropy has to be absorbed by the electronic entropy, the nuclear entropy may significantly reduce the lowest achievable temperature T_{base}. However, to our knowledge, this problem has not yet been addressed. In order to get an idea about the relevance of this problem, we estimated the total entropy S_{total} including the nuclear part. The analysis of the field and temperature dependence of this total entropy indicates that the effect of the nuclear contribution is negligible for base temperatures above 200

mK but starts to become relevant below 200 mK and can be strongly relevant below 100 mK, limiting T_{base} to values well above those determined from the electronic entropy only. However, since the nuclear contribution is strongly material-dependent, a simple general statement is not possible. The landscape of the total entropy $S_{total}(T, B)$ as colour-coded in Fig. 4a is discussed in detail in Supplementary Note 7.

The change of the entropy per volume $-\Delta S^{v}$ is of particular interest for practical cooling systems (Fig. 3b). It directly describes the heat released from a refrigerant per unit volume during isothermal magnetisation, and the entropy to be reabsorbed during the subsequent demagnetisation. In order to determine $-\Delta S^{v}$ for $YbNi_{1.6}Sn$, $S^{v}_{total}(8\,T)$ is subtracted from $S^{v}_{total}(0\,T)$. Since only the processed electronic entropy is published for $Yb_{0.81}Sc_{0.19}Co_2Zn_{20}$ (ref. 14), a direct comparison of S_{total} is not possible. Here, $-\Delta S^{v}$ is calculated as $S^{v}_{elec}(8\,T) - S^{v}_{elec}(0\,T)$.

Importantly, the volumetric entropy density change $-\Delta S^{v}$ of $YbNi_{1.6}Sn$ at 1.4 K is at least a factor of 2.5 higher than that of the commonly used hydrated insulating refrigerants chromium potassium alum (CPA) and ferric ammonium alum (FAA)[8,12]. It stays larger to temperatures as low as 230 mK. A more extensive comparison with state-of-the-art magnetocaloric materials for sub 350 mK ADR is discussed in Supplementary Note 8. $YbNi_{1.6}Sn$'s extreme entropy density enables a dramatic saving in the size of the magnet required for this cooling method, which in turn helps shrink the system as a whole. The resulting miniaturisation is important in weight critical applications such as deployment of quantum sensors on satellites or other mobile platforms, and it offers new design possibilities for multistage cooling systems. Small cooling systems can also be shielded more straightforwardly from external environmental influences (such as parasitic heat loads, vibrations or radiation), and they enable faster turn-around times because less equipment has to be (pre-)cooled, while maintaining the same cooling capacity at lowest temperature.

The dilution of magnetic Yb^{3+} ions to suppress T_m, as in the tuned system $Yb_{0.81}Sc_{0.19}Co_2Zn_{20}$, strongly reduces the entropic capacity change $-\Delta S^{v}$ (Fig. 3b). This, together with the challenge of growing sufficiently large single crystals, limits the application potential of this interesting super-heavy electron system.

Performance of $YbNi_{1.6}Sn$ in an adiabatic demagnetisation refrigerator. The practical performance of magnetocaloric materials can in principle be predicted from the experimentally determined entropy landscape $S_{total}(T, B)$, which usually requires measuring $C(T)$ in various fixed applied magnetic fields (more details in Supplementary Note 7). Alternatively, the T dependence of the magnetisation $M(T)$ at fixed field can be used via the Maxwell relation: $\left(\partial S/\partial B\right)_T = \mu_0\left(\partial M/\partial T\right)_B$. These measurements are time consuming and additional extrapolations or estimates of the form of the entropy at lowest T may still have to be made. Therefore, we complement the thermodynamic measurements in $YbNi_{1.6}Sn$ with a set-up for directly testing the practical performance of $YbNi_{1.6}Sn$ in a prototype ADR cooling module. Our module contains approximately 15 g of $YbNi_{1.6}Sn$ powder compressed into a thin-walled brass can. A calibrated RuO_2 thermometer and a thin film resistive heater are mounted on the top of the brass can. Further information on our engineering model and the typical procedure to perform a magnetic cool-down can be found in Supplementary Note 9.

The temperature-field trajectories for two demagnetisation runs are shown in Fig. 4a. These trajectories can be compared against the isentropic line expected from the experimentally determined entropy landscape (solid grey line in Fig. 4a, Supplementary Note 7). The discrepancies between the experimental trajectories and computed isentrope highlight the importance of cross-checking entropy calculations with demagnetisation experiments. The higher temperature measured in the ADR runs could indicate parasitic material that needs to be cooled down as well. Our simple ADR module is a prototype only. It is designed to perform feasibility tests. In turn, the computed entropy landscape relies on extrapolations of both nuclear and electronic heat capacity below the minimum temperature at which heat capacity could be obtained. If we take the measured trajectories as closely approximating the actual isentrope for $YbNi_{1.6}Sn$ it implies that our current assumption of $(C_{elec}(T)/T \xrightarrow{T\to 0} 0)$ might not reflect the accurate physics in weakly interacting local moment systems. Further measurements deep below the currently accessible temperature range will be required to decide the fundamental question regarding the correct description of $YbNi_{1.6}Sn$ at ultra-low temperatures.

Test run results time-dependently recorded on our demonstrator module are summarised in Fig. 4b, for a starting temperature $T_{bath} = 1.8$ K and applied fields of 4 T, 9 T and 14 T. More detailed information about the demonstrator performance for a wider range of starting fields, temperatures and heat loads are provided in Supplementary Note 10. Different demagnetising rates $\dot{B}$ do not affect the base temperatures, which indicates that eddy current heating is negligible, as suggested by prior estimates (Supplementary Note 11). The heat leak Φ into the low T stage can be estimated from the known heat capacity and the warming rate to be less than 0.4 μW. The minimum measured base temperature of 116 mK occurs at the largest field reduction (14 T → 0 T). An intermediate starting field of 4 T produced $T_{base} \approx 240$ mK. To the best of our knowledge, experiments with similar set-ups in identical cryostat have been described previously only on three other

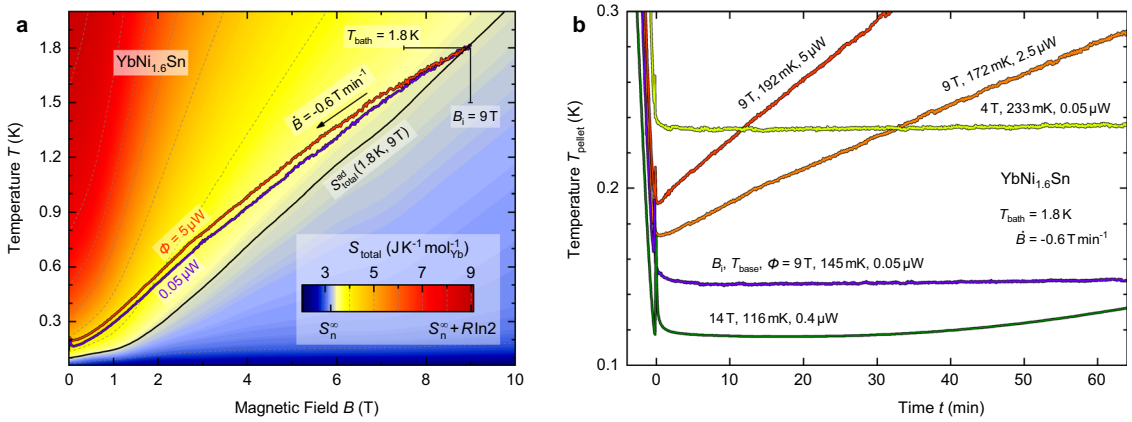

Fig. 4 | Magnetocaloric cooling. Temperature profiles of a test module containing about 15 g pressed $YbNi_{1.6}Sn$. **a** Starting at ($T_{bath} = 1.8$ K, $B_i = 9$ T) two temperature-field trajectories of measured demagnetisation runs with different heat loads Φ result in T_{base} of 145 mK and 192 mK, respectively. The background colour-codes the entropy landscape $S_{total}(T, B)$. The adiabatic contour cutting 1.8 K and 9 T is emphasised as dark grey line S^{ad}_{total}. **b** After full demagnetisation the $YbNi_{1.6}Sn$ pellet's temperature tends towards T_{bath} again. The observed substantial hold times even under high heat loads demonstrate the large entropy capacity of $YbNi_{1.6}Sn$. The heating curves labelled $\Phi \le 0.4$ μW have been recorded without added heater power. The parasitic heat load in this case is estimated from $C(T)\dot{T}$. Additional heat loads ($\Phi \ge 2.5$ μW) were applied using a resistive heater.

materials: (i) the similar material $YbPt_2Sn$ reached a base temperature of roughly 0.16 K and a hold-time below 350 mK of about 160 min under the initial conditions of $T_{bath} = 1.8$ K and $B_i = 7$ T (ref. 13). (ii) $YbCu_4Ni$[35] reached a base temperature of 0.2 K, larger than 140 mK achieved with $YbNi_{1.6}Sn$. This is possibly because the entropy profile is not as sharp as the one of $YbNi_{1.6}Sn$ below 2 K. In fact, at 2K the entropy of $YbNi_{1.6}Sn$ is about 6 $JK^{-1}mol^{-1}$ ($>R \ln 2$) while for $YbCu_4Ni$ it is just above 4 $JK^{-1}mol^{-1}$, i.e., still well below $R \ln 2$. The Kondo temperature in $YbCu_4Ni$ has been estimated to be < 2 K[36], and it shows magnetic ordering only below 170 mK[24]. The Kondo temperature in $YbCu_4Ni$ can be determined from the electrical resistance, which shows a Kondo coherence maximum at about 0.3 K. This implies $T_K < 0.3$ K. Consequently, $YbCu_4Ni$ is located in the local moment limit to the left side of Fig. 1a. In $YbNi_{1.6}Sn$, no Kondo scattering has been observed in resistivity measurements. (iii) For the insulating Yb-based frustrated magnet $KBaYb(BO_3)_2$ a T_{base} of around 40 mK has been reported ($T_{bath} = 2$ K, $B_i = 5$ T). Here, the hold-time below 350 mK was 40 min[37]. Although hold-times are only comparable to a limited extent (due to different experimental conditions, for example Φ), $YbNi_{1.6}Sn$'s time in the above mentioned 4 T—run is more than 420 min and thus multiple times larger than in the reference compounds[13,37]. This is in excellent agreement with predictions based on entropy densities (Supplementary Note 8).

When a heater is used to simulate large heat loads of 2.5 μW or 5 μW, the $YbNi_{1.6}Sn$ ADR operates in temperature ranges that are still below those of a typical ^{3}He cryostat ($T_{base} < 350$ mK). The immense entropy capacity $-\Delta S^v$ (Fig. 3) and intrinsically high thermal conductivity in $YbNi_{1.6}Sn$ therefore lead to high cooling power and long hold-time at practically important base temperatures, the three central requirements for a useful refrigerant material.

Conclusions

The intermetallic $YbNi_{1.6}Sn$ emerges as a superior magnetocaloric for attaining sub-Kelvin temperatures in adiabatic demagnetisation refrigeration, because (i) its high entropy density, effective heat absorption, good chemical stability, UHV bakeability and high thermal conductivity are key advantages over traditional insulating magnetocalorics such as CPA and FAA; (ii) it shows a strong magnetocaloric effect and weak signatures of magnetic order at ultra-low temperatures; (iii) it does not require the expensive noble metals Pd and Pt that are needed to produce otherwise comparable metallic magnetocalorics such as $YbPt_2Sn$, $YbPt_2In$, $YbPd_2Sn$ and $YbPd_2In$, allowing a significant reduction in the cost of raw materials.

Further improved entropy density may be possible in materials with a more highly degenerate CEF ground state than the doublet found in $YbNi_{1.6}Sn$ and other (quasi) 1-2-1 magnetocalorics. As a standalone refrigerant, $YbNi_{1.6}Sn$ offers good cooling power and long hold times to the 150 mK temperature range and thereby provides an attractive alternative to ^{3}He refrigerators. Its use can be extended into the 10 mK temperature range by combining it with paramagnetic salts such as CPA or a $PrNi_5$ nuclear demagnetisation stage in a dual system[8].

Methods

Material preparation and characterisation

Because of the huge difference in the melting points of the pure elements ($T_{Ni} \approx 1730$ K,$T_{Yb}T_{Yb} \approx 1100$ K and $T_{Sn} \approx 500$ K), we prepared the polycrystalline samples in a two-stage arc-melting process under ultrapure argon atmosphere. In a first stage an appropriate amount of Yb and of the low-melting element Sn was melted to a small button. In the second step different proportions of Ni were added and melted with the pre-reacted YbSn mixture. The optimal weight ratio was determined to be 0.4 Ni : 1 YbSn. In this step, the samples were repeatedly melted and turned over to enhance homogeneity. The total weight loss after the whole procedure was about 4 wt%. This can be attributed to the evaporation of Yb due to its low boiling point of 1469 K. An excess of 8% to 14% Yb was used in the initial composition to compensate for this loss. We deliberately chose a rather simple sample preparation technique which can easily be adapted for a larger scale industrial production at reasonable cost. This limits the achievable phase purity, which is, however, completely sufficient for the purpose of adiabatic cooling.

Chemical characterisation

We employed a differential scanning calorimeter (PerkinElmer DSC 8500) to obtain the differential scanning calorimetry data at temperatures between 300 K and 1500 K. The energy-dispersive X-ray (EDX) spectroscopy at room temperature was performed on a scanning electron microscope Philips XL30. Room temperature X-ray powder diffraction data were recorded on a STOE Stadip instrument in transmission mode using Cu $K\alpha 1$ radiation. The lattice parameters refinement by least-squares fitting as well as Rietveld refinements have been done using the programme package FULLPROF.

Physical characterisation

Specific heat and electrical resistivity in the temperature range 400 mK < T < 400 K were measured in a commercial Quantum Design (QD) PPMS equipped with a ^{3}He option. The specific heat in the millikelvin regime range down to around 90 mK was determined with a relaxation method in a ^{3}He/^{4}He dilution refrigerator (Oxford Instruments) using a compensated heat pulse method[38]. The magnetic properties above 1.8 K were measured using a QD SQUID VSM.

ADR set-up

We have constructed a simple ADR test set-up for the QD PPMS. The set-up, as sketched in Supplement Note 9, comprises primarily of a brass-enclosed pressed $YbNi_{1.6}Sn$ powder pill, calibrated RuO_2 thermometer, a 200 Ω thin-film resistor as heater, a thin-wall plastic tube as thermally insulating support, a PPMS Helium-4 blank puck and a brass heat shield. Superconducting NbTi wires in CuNi shield are used as current and voltage leads for the heater and thermometer to ensure minimal heat leak to the cold stage. Before reaching the heater and thermometer, the wires are wrapped around and glued down with GE varnish to the outer surface of the pressed pill brass enclosure, minimising thermal gradient between the thermometer and the coolant. Further details on measuring the magnetocaloric effect are given in Supplementary Note 9.

Data availability

All data needed to evaluate the conclusions in the paper are present in the paper and its supplement as well as in the Data Repository at the University of Cambridge. It can be downloaded form ref. 39.

Received: 8 February 2022; Accepted: 5 April 2024;
Published online: 26 April 2024

References

1. Tuoriniemi, J. Physics at its coolest. *Nat. Phys.* **12**, 11–14 (2016).
2. Moldover, M. R., Tew, W. L. & Yoon, H. W. Advances in thermometry. *Nat. Phys.* **12**, 7–11 (2016).
3. Katori, H. Optical lattice clocks and quantum metrology. *Nat. Photonics* **5**, 203–210 (2011).
4. Ladd, T. D. et al. Quantum computers. *Nature* **464**, 45–53 (2010).
5. Nowogrodzki, A. The world's strongest MRI machines are pushing human imaging to new limits. *Nature* **563**, 24–26 (2018).
6. Lamarre, J.-M. et al. *Planck* pre-launch status: The HFI instrument, from specification to actual performance. *Astronomy Astrophys.* **520**, A9 (2010).
7. Schmetz, J. et al. An introduction to meteosat second generation (MSG). *Bull. Am. Meteorol. Soc.* **83**, 977–992 (2002).
8. Pobell, F. *Matter and Methods at Low Temperatures* (Springer-Verlag Berlin Heidelberg, 2007).
9. Debye, P. Einige Bemerkungen zur Magnetisierung bei tiefer Temperatur. *Annalen der Physik* **386**, 1154–1160 (1926).

10. Giauque, W. F. A thermodynamic treatment of certain magnetic effects. A proposed method of producing temperatures considerably below 1° absolute. *J. Am. Chem. Soc.* **49**, 1864–1870 (1927).
11. Kürti, N. & Simon, F. Production of very low temperatures by the magnetic method: Supraconductivity of cadmium. *Nature* **133**, 907–908 (1934).
12. Wikus, P., Canavan, E., Heine, S. T., Matsumoto, K. & Numazawa, T. Magnetocaloric materials and the optimization of cooling power density. *Cryogenics* **62**, 150–162 (2014).
13. Jang, D. et al. Large magnetocaloric effect and adiabatic demagnetization refrigeration with $YbPt_2Sn$. *Nat. Commun.* **6**, 8680 (2015).
14. Tokiwa, Y. et al. Super-heavy electron material as metallic refrigerant for adiabatic demagnetization cooling. *Sci. Adv.* **2**, e1600835 (2016).
15. Doniach, S. The Kondo lattice and weak antiferromagnetism. *Physica B+C* **91**, 231 – 234 (1977).
16. Coleman, P. & Schofield, A. J. Quantum criticality. *Nature* **433**, 226–229 (2005).
17. Senthil, T., Sachdev, S. & Vojta, M. Fractionalized fermi liquids. *Phys. Rev. Lett.* **90**, 216403 (2003).
18. Vojta, M. Orbital-selective mott transitions: Heavy fermions and beyond. *J. Low Temp. Phys.* **161**, 203–232 (2010).
19. Coleman, P. Local moment physics in heavy electron systems. *AIP Conf. Proc.* **629**, 79–160 (2002).
20. Ramirez, A. P. Strongly geometrically frustrated magnets. *Ann. Rev. Mater. Sci.* **24**, 453–480 (1994).
21. Aoki, Y., Sato, H. R., Sugawara, H. & Sato, H. Anomalous magnetic properties of Heusler superconductor $YbPd_2Sn$. *Phys. C: Superconductivity* **333**, 187–194 (2000).
22. Gastaldo, F. et al. $YbPd_2In$: A promising candidate for strong entropy accumulation at very low temperature. *Phys. Rev. B* **100**, 174422 (2019).
23. Gruner, T. et al. Unusual weak magnetic exchange in two different structure types: $YbPt_2Sn$ and $YbPt_2In$. *J. Phys.: Condensed Matter* **26**, 485002 (2014).
24. Sereni, J. G., Čurlík, I., Giovannini, M., Strydom, A. & Reiffers, M. Physical properties of the magnetically frustrated very-heavy-fermion compound $YbCu_4Ni$. *Phys. Rev. B* **98**, 094420 (2018).
25. Kurita, N. et al. Thermal and magnetic properties of the low-temperature antiferromagnet $Ce_4Pt_{12}Sn_{25}$. *Phys. Rev. B* **82**, 174426 (2010).
26. Skolozdra, R. V. & Komarovskaya, L. P. Crystal structures of the compounds $LuNi_2Sn$, $YbNi_2Sn$ and $LuNi_4Sn$. *Ukrains'kii Fizichnii Zhurnal (Ukrainian Edition)* **28**, 1093–1095 (1983).
27. Shirron, P. J. Cooling capabilities of adiabatic demagnetization refrigerators. *J. Low Temp. Phys.* **148**, 915–920 (2007).
28. Bartlett, J., Hardy, G. & Hepburn, I. D. Design and performance of a fast thermal response miniature Chromium Potassium Alum (CPA) salt pill for use in a millikelvin cryocooler. *Cryogenics* **65**, 26–37 (2015).
29. Desgranges, H.-U. & Schotte, K.-D. Specific-heat of the Kondo Model. *Phys. Lett. A* **91**, 240–242 (1982).
30. Sereni, J. G. Thermomagnetic properties of very heavy fermions suitable for adiabatic demagnetisation refrigeration at low temperature. *Philos. Mag.* **100**, 1211–1225 (2020).
31. Banda, J. et al. Electronuclear quantum criticality. Preprint at https://arxiv.org/abs/2308.15294 (2023).
32. Carretta, P., Pasero, R., Giovannini, M. & Baines, C. Magnetic-field-induced crossover from non-fermi to fermi liquid at the quantum critical point of $YbCu_{5-x}Au_x$. *Phys. Rev. B* **79**, 020401 (2009).
33. Čurlík, I. et al. Extremely high density of magnetic excitations at $T = 0$ in $YbCu_{5-x}Au_x$. *Phys. Rev. B* **90**, 224409 (2014).
34. Banda, J.*Thermodynamic studies of non-Kondo Ce- and Yb-based intermetallics*. Ph.D. thesis, Technical University of Dresden, Germany (2021).
35. Shimura, Y. et al. Magnetic refrigeration down to 0.2 K by heavy fermion metal $YbCu_4Ni$. *J. Appl. Phys.* **131**, 013903 (2022).
36. Čurlik, I., Mát'ošová, Š., Il'kovič, Š., Reiffers, M. & Giovannini, M. Transport and magnetic properties of $YbCu_4Ni$. *Acta Phys. Polonica A* **122**, 6 (2012).
37. Tokiwa, Y. et al. Frustrated magnet for adiabatic demagnetization cooling to milli-Kelvin temperatures. *Commun. Mater.* **2**, 42 (2021).
38. Wilhelm, H., Lühmann, T., Rus, T. & Steglich, F. A compensated heat-pulse calorimeter for low temperatures. *Rev. Sci. Instruments* **75**, 2700–2705 (2004).
39. Link to Data Repository at the University of Cambridge; https://doi.org/10.17863/CAM.106770.

Acknowledgements

This work was supported by the EPSRC of the UK through grant EP/P023290/1. T.G. acknowledges support by the Alexander von Humboldt Foundation within the Feodor Lynen Research Fellowship and by Darwin College (Cambridge, UK). We are indebted to J.G. Sereni, I. Hepburn and R. Temirov for useful discussions. Moreover, we thank M. Baenitz and R. Hempel-Weber.

Author contributions

F.M.G., C.G. and T.G. conceived the research. T.G. synthesised the samples and conducted characterisation and specific heat measurements down to 400 mK. J.B., D.J. and M.B. performed low-temperature specific heat experiments. J.C. designed and fabricated the ADR test set-up. All authors contributed to data analysis and interpretation. T.G. and F.M.G. wrote the manuscript with inputs from all other authors.

Competing interests

The authors declare no competing interests.

Additional information

Supplementary information The online version contains supplementary material available at https://doi.org/10.1038/s43246-024-00494-4.

Correspondence and requests for materials should be addressed to Thomas Gruner or F. Malte Grosche.

Peer review information *Communications Materials* thanks the anonymous reviewers for their contribution to the peer review of this work. Primary Handling Editor: Aldo Isidori.